Journal of Manufacturing Processes 150 (2025) 407–415

Contents lists available at ScienceDirect

Journal of Manufacturing Processes

journal homepage: www.elsevier.com/locate/manpro

Research article

Spatial-terminal iterative learning control for registration error elimination in roll-to-roll gravure printing systems

Zifeng Wang [a], Jingyang Yan [b], Rui Ma [b], Xian Du [b], Xiaoning Jin [a,*]

[a] Department of Mechanical and Industrial Engineering, Northeastern University, 360 Huntington Avenue, Boston, 02215, MA, USA
[b] Mechanical and Industrial Engineering Department, Institute for Applied Life Sciences, University of Massachusetts, Amherst, 120 Tillson Farm Road, Amherst, 01003-9346, MA, USA

ARTICLE INFO

Keywords:
Iterative learning control (ILC)
Advanced manufacturing
Roll-to-roll (R2R) printing process
Registration error

ABSTRACT

Roll-to-roll (R2R) printing techniques are promising for high-volume continuous production of flexible printed electronics. One of the major challenges in R2R flexible electronics printing is achieving high-precision registration control when transient disturbances repeatedly occur during the printing process. Conventional registration control strategies often rely on real-time feedback controllers, such as PID control, to regulate web tension and velocity. However, these approaches do not guarantee convergence of the registration error to zero. This paper introduces a Spatial-Terminal Iterative Learning Control (STILC) method, designed to iteratively reduce the registration error to an undetectable level. The proposed STILC approach holds the control input constant during one operation cycle and updates the control input profile for the next operation cycle, without requiring real-time monitoring. The effectiveness of the proposed STILC is validated by numerical simulations and experiments on a lab-scale R2R gravure printing system. The experimental results show that the registration errors are reduced to an undetectable range after a reasonable number of iterations when the proposed STILC is applied, which demonstrates that the STILC method is effective for high-precision registration control in R2R printing and is generalizable to manufacturing processes involving highly repetitive transient operations.

1. Introduction

Roll-to-roll (R2R) printing systems have emerged as a promising manufacturing technology that facilitates high-throughput and continuous manufacturing for various flexible-substrate-based products, such as thin-film printing electronic devices, batteries, and solar cells, among others [1–7]. For example, Zuo et al. have demonstrated scalable manufacturing methods for 2D perovskite solar cells by developing both a facile drop-casting screening approach to identify optimal formulations and implementing the process via roll-to-roll slot-die coating on flexible substrates, achieving power conversion efficiencies of 8.0–8.8% without requiring conventional spin-coating methods [6,7]. In the practical production of R2R gravure printing processes, the registration error is a vital concern that significantly impacts the quality and functionality of the final products [8,9]. Registration error refers to the misalignment between the desired positions and the real printed positions of printed patterns on the substrate. This misalignment must be effectively controlled to meet stringent tolerance requirements to guarantee the functionality of products. However, measuring the registration error is only feasible after the complete pattern has been printed, making real-time monitoring infeasible during the printing cycle [10,11]. The lack of continuous detectable signals adds to the challenge of controlling registration errors.

This control challenge is further exacerbated by transient disturbances in system states, such as web tensions and web speeds [12–15], where the term *web* refers to the flexible substrate in the context of R2R industries. One significant consequence of these transient disturbances is *web slippage*, a phenomenon that is directly caused by fluctuations in web tensions and web speeds [16]. Web slippage stands out as a primary contribution to registration errors in R2R printing processes [17]. Since web tensions and speeds can be continuously monitored by sensors and accessed by controllers in real-time, several feedback control methods have been introduced to address this challenge. Model Predictive Control (MPC) for tension feedback control and PID control methods have been developed towards minimizing registration errors by precisely regulating the crucial variables within R2R printing systems [13,18–21]. However, the traditional feedback control methods have shown limitations in fully addressing this issue. Even if feedback controllers can make the tensions and speeds converge to their reference values at the end of each printing cycle, the registration error for each cycle cannot be completely eliminated. This is due to the

* Corresponding author.
E-mail address: xi.jin@northeastern.edu (X. Jin).

https://doi.org/10.1016/j.jmapro.2025.06.004
Received 9 April 2025; Received in revised form 26 May 2025; Accepted 2 June 2025
Available online 23 June 2025

cumulative nature of the measurement, which is evaluated at the end of each cycle. This cumulative measurement of the output variable at the termination of each operation cycle is referred to as the *terminal output* for that specific cycle. In an R2R system, disturbances often occur repeatedly due to the cyclic nature of its rotating components. This leads to a repetitive registration error for each printing cycle. In scenarios requiring high-precision printing registration control, these feedback control methods might prove inadequate.

Iterative learning control (ILC) stands out as an effective method for controlling repetitive manufacturing processes by compensating disturbances in a feedforward manner [22,23]. In some previous studies [24,25], ILC methods were designed to mitigate transient behaviors in R2R processes by iteratively regulating web tensions. However, these methods require prior knowledge of the desired tension profile for each cycle. In practice, it is more reasonable for applications to tolerate slight deviations in tensions during the cycle while closely monitoring the registration error, which is the terminal output [26,27]. Terminal Iterative Learning Control (TILC) methods have been developed to update the control input profile iteratively based on only the terminal output, rather than the entire output profile [28–30]. In TILC, the input profile for the current iteration is determined by the terminal output of the previous iteration and a predefined basis function. In [31], a basis function is designed based on a state-space model of a Rapid Thermal Processing Chemical Vapor Deposition (RTPCVD) system. More complicated basis functions can be found in [28–30], utilizing data-driven techniques to tackle complex systems without sufficient prior knowledge. To select a proper pre-defined basis function for a specific control problem, practitioners need to make the best use of the prior knowledge of the system while also limiting the complexity of the function to ensure it can be implemented in real-world hardware. In this work, we know from the modeling analysis that web slippage can be suppressed by reducing the maximum difference between the motor torques of unwinding and rewinding rollers. That is, the motor torque can remain constant during a single printing cycle, but it can be adjusted cycle-by-cycle iteratively based on the measurement of slippage. Therefore, we select a constant-value basis function for the TILC-based method proposed in Section 3 based on the characteristics of the R2R gravure printing process. This approach could be a practical choice for many industrial production processes where control input variables cannot be frequently or flexibly adjusted. In such cases, maintaining certain state variables within an acceptable range may lead to good quality outcomes, rather than aiming for a specific desired profile. Designing a usable heuristic constant profile within a few trials is typically not challenging. In our study, this constant-value basis function effectively deals with registration errors caused by web slippage, while keeping the computational burden to a minimum. Particularly, we address the period mismatch problem for the mismatch between the registration error sensing period and the control iteration length by defining a special terminal function for each control iteration.

Another challenge for applying ILC methods to the R2R registration error control problem is that the angle-periodic disturbance is not repeated over a fixed time period, which must be satisfied to guarantee the effectiveness of traditional ILC methods. To address this, the concept of Spatial Iterative Learning Control (SILC) has been proposed and successfully demonstrated in various applications, including motor torque control [32], additive manufacturing processes [33–36], wind turbines [37], and multi-axis linear motion stages [23,38]. SILC introduces an iterative updating law constructed in the spatial domain, expanding the capabilities of iterative learning through an alternative definition of *iteration*. Different techniques, such as Crank–Nicholson discretization [39,40] and 2-D spatial convolution [33–35], are used to capture the system dynamics and design ILC updating law in the spatial domain. Zhang et al. proposed a layered-and-subregional model-free adaptive iterative learning control (LS-MFAILC) method for laser additive manufacturing that addresses intra-layer instability by dividing each layer into multiple regions and adaptively controlling process parameters using thermal melt pool information [36]. In this paper, we propose a new approach called Spatial-Terminal ILC (STILC) that combines the strengths of SILC and TILC. This approach is designed to address the distinctive challenges inherent in controlling registration errors within R2R gravure printing. Our another work [41] has validated a similar STILC strategy for eliminating the RE in a double-layer pattern in a two-printing-roller R2R process by numerical simulation. In this work, the proposed STILC approach can attenuate the registration error and maintain the registration error within the undetectable range for the image-based sensor after 8–10 iterations in the experiments. Due to its foundation in TILC-based principles, STILC only requires the terminal output from each iteration to update the input profile, where *iteration* corresponds to a single rotational cycle of the printing component. Thus, it can work in R2R registration control problems without continuous-time monitoring of the registration error or any other measurements. Furthermore, the proposed STILC method can handle the angle-periodic disturbance in R2R system since it is designed in the spatial domain rather than the time domain. The mathematical analysis proves its stability in the iteration domain. To demonstrate the effectiveness of the STILC method in our R2R registration control problem, we apply the proposed STILC approach in a lab-scale R2R gravure printing testbed. The image acquisition system, in conjunction with a closed-loop feedback registration algorithm [42], diligently measures the registration error stemming from iterative web slippage. The experimental results demonstrate that the proposed STILC approach effectively suppresses the registration error induced by angle-periodic transient disturbances, reducing it to an undetectable level.

The main contributions of this work are listed below:

(1) A spatial domain TILC approach, specifically the STILC, is designed to address the registration error in R2R gravure printing systems. By iteratively learning the appropriate control actions from cycle-by-cycle measurements of registration errors and past actions, this TILC-based method effectively addresses angle-periodic transient disturbances and reduces the demand for control rate and high-performance hardware.

(2) The effectiveness of the STILC method is theoretically validated through stability analysis, demonstrating that the registration error corresponds with the analytically derived impact of web slippage.

(3) The proposed STILC approach is implemented in a lab-scale R2R gravure printing system and demonstrates practical effectiveness in real-world manufacturing applications.

The remainder of this paper is organized as follows: Section 2 establishes the physics-based model of the R2R gravure printing system and the registration error caused by the angle-periodic disturbance. In Section 3, the novel STILC method is designed and its stability is analyzed in the iteration domain. Section 4 describes the experimental setup and analyzes the experimental results to validate the effectiveness of the proposed STILC in real-world applications. Section 5 concludes the paper.

2. Problem formulation

This section establishes the dynamic model of the gravure printing system with one unwinding roller, one rewinding roller, and one gravure printing roller, which is consistent with our experimental setup. Subsequently, the mechanism of registration error caused by transient web tension fluctuations is derived. This derivation corresponds to the statement in the introduction that web slippage is primarily caused by variations in web tension and web speed.

2.1. R2R process modeling

A typical R2R printing system includes a web handling system transporting the flexible web (substrate) through a series of rollers. In this paper, we study a streamlined R2R printing system with one

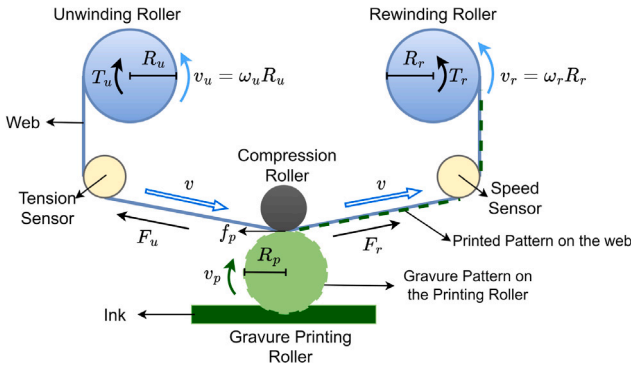

Fig. 1. Schematic illustration of a streamlined R2R gravure printing system consisting of three essential components: an unwinding roller that supplies the flexible substrate, a central gravure printing roller that transfers the printed pattern while maintaining a constant rotation speed v_p, and a rewinding roller that collects the printed substrate. The system operates with carefully balanced opposing motor torques ($T_u = -T_r$) to maintain consistent web tension throughout the printing process, while the web speed v matches the printing roller speed to ensure precise pattern transfer without slippage between the substrate and rollers.

unwinding roller, one rewinding roller, and one gravure printing roller. The streamlined R2R gravure printing system is shown in Fig. 1.

When the system is running at a steady state, the gravure printing roller maintains a constant rotating speed v_p, and the web speed v keeps consistent with v_p, i.e. $v = v_p$. To maintain a constant tension in the web, the motor torques of unwinding and rewinding rollers are set as opposite but the same absolute value, i.e. $T_u = -T_r$, where T_u is the unwinding roller motor torque and T_r is the rewinding roller motor torque. In this work, we have the following idealized assumptions for the purpose of approximation and simplification:

Assumption 1. The web elongation caused by tension stretching is relatively small. Thus, we can neglect the impact of web deformation.

Assumption 2. There is no slippage between the unwinding or rewinding rollers and the web, since the web is tightly wrapped on the rollers.

With Assumptions 1 and 2, we can approximately assume the speed of the web is consistent at any point along the web, i.e., $v_u = v = v_r$, where v_u and v_r are the tangential speeds of unwinding and rewinding rollers, respectively.

Assumption 3. As the R2R system is running, the web is being transported from the unwinding roller to the rewinding roller. Thus, the web volumes wrapping on these two rollers are continuously changing. As a result, the radii of the unwinding and rewinding rollers, R_u and R_r, are also continuously varying. However, the thickness of the web is relatively small compared to the size of rollers. Thus, the radius variations of unwinding and rewinding rollers can be neglected, i.e., R_u and R_r are constant.

With Assumptions 1–3, we have

$$\omega_u R_u = v = \omega_r R_r \tag{1}$$

where ω_u and ω_r are the angular speeds of the unwinding and rewinding rollers, respectively.

Based on Newton's Second Law, we can get the dynamic equations for the unwinding and rewinding rollers

$$\begin{aligned} F_u R_u - T_u &= J_u \frac{\dot{v}}{R_u} \\ T_r - F_r R_r &= J_r \frac{\dot{v}}{R_r} \end{aligned} \tag{2}$$

where F_u and F_r are the stretching forces that the web applies to the unwinding and rewinding rollers, and J_u and J_r are the inertia of the unwinding and rewinding rollers. The inertia of the tension sensor and the speed sensor are relatively small to avoid affecting the measurements significantly. Thus, we can assume the tension is consistent in the web between the unwinding and rewinding rollers, i.e. $F = |F_u| = |F_r|$, where F is the web tension force. Since the tension sensor and the speed sensor do not apply any force to the web along the longitudinal direction of the web, there are three forces applied to the web in total. Other than the reaction forces of F_u and F_r, the gravure printing roller also applies a friction force to the web. When the difference between F_u and F_r does not exceed the maximum static friction force between the web and the gravure printing roller surface, the gravure printing roller can provide sufficient friction force to hold the web at the contacting point. In this occasion, the web speed v is mastered by the gravure printing roller and no slippage phenomenon occurs. The force equilibrium equation is given as

$$F_u + f_p = F_r \tag{3}$$

where f_p is the friction force between the gravure printing roller and the web. To avoid slippage, f_p should be less than the maximum static friction $\bar{f}_s$.

Assumption 4. The friction force does not change its direction during an iteration.

Assumption 4 holds because the unwinding roller and the rewinding roller are both motorized under specified torque profiles, and their torques are applied in opposite directions in the experimental setup to generate tension throughout the web. When positive disturbances are introduced to the rewinding roller, the unwinding roller torque becomes insufficient to maintain the web's tension equilibrium. The friction between the web and printing roller compensates for this imbalance, and slippage occurs if the friction is insufficient to restore equilibrium. Therefore, the friction consistently acts to resist the web's acceleration towards the rewinding roller, establishing an invariant direction for the friction force.

2.2. Registration error caused by transient disturbances

Transient disturbances in the R2R system may break the equilibrium in (3). If the difference between F_u and F_r exceeds the maximum static friction force, the slippage will occur between the web and the gravure printing roller, and the friction will become dynamic friction. The friction force f_p can be described as below:

$$f_p = \frac{v - v_p}{|v - v_p|} f_d \tag{4}$$

where f_d is the constant value of dynamic friction.

The registration error caused by slippage is defined as the difference between the correct pitch length and the real pitch length of the printed pattern as illustrated in Fig. 2. It can be derived by the following integral:

$$e = \int_{t_s}^{t_e} (v - v_p) dt + w \tag{5}$$

where e denotes the registration error, t_s and t_e are the start and end time of one complete printing cycle, and w is the uncertainty introduced by the registration error measurement, which is decided by the precision of the image-based sensor in this study. The gravure printing roller prints every complete pattern by rotating over a complete cycle (0–360 degree). To simulate the slippage-caused registration error, we introduce an angle-periodic disturbance to the rewinding roller motor torque. Transient torque disturbances linked to the rotational dynamics of motors are common across various applications arising from model mismatches [43], vibrations [44], or intrinsic motor hardware imperfections [45]. For example, cogging torque, attributed to roundness

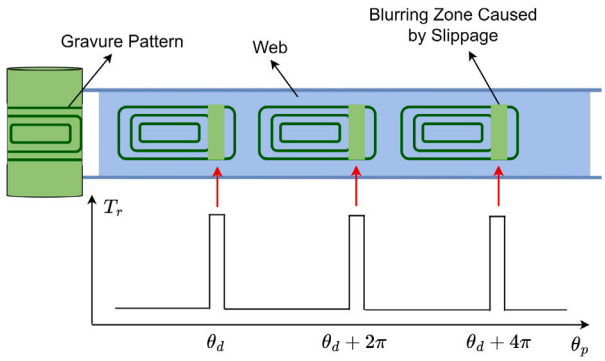

Fig. 2. Registration error caused by the slippage phenomenon.

errors, is a common source of angle-periodic impulse disturbances. An impulse occurs repetitively every time the rewinding roller rotates to the same angular phase. In this work, we assume that the registration error can only be measured at the end of each printing cycle by an image-based sensor. It is worth noting that there exists a mismatch between the angle-based disturbance period and the registration error sensing period due to the different roller radii. In this study, the unwinding and rewinding rollers have the same radius, which is 3.81 times of the radius of the gravure printing roller. Therefore, by defining an iteration as a rotation cycle of the rewinding roller, we have an iteration-invariant disturbance profile and three registration error measurements in each iteration. One solution for the period mismatch issue in ILC design is to construct a Point-to-Point (P2P) ILC [46,47], which tracks a point-wise desired trajectory instead of a continuous one. However, in this work, our target is even simpler than tracking a point-wise desired trajectory: we aim to eliminate any registration error measured during an iteration. Therefore, we design a terminal output function that picks the registration error measurement with the largest absolute value during an iteration as the terminal output. By applying this terminal output function, we can construct a TILC framework to update the control input profile iteratively. The control goal is to adjust the input of unwinding roller motor torque T_u based on the registration error measurement to eliminate the registration error after a few iterations.

3. STILC design and analysis

3.1. STILC design

In the analysis in Section 2, we know the slippage occurs when the difference between the upstream tension force F_u and the downstream tension force F_r exceeds the maximum static friction. The repetitive impulse disturbance introduced to the rewinding roller motor torque will make this difference exceed the maximum static friction in a short time during each printing cycle. The ideal control is to maintain the upstream tension force equal to the downstream tension force in all time. However, there is not always sufficient sensing capability of measuring real-time web tensions between any web span in practical R2R systems. Therefore, it is important that our STILC method can update the control input variable (T_u) for each printing cycle, utilizing only the registration error measurement at the completion of the preceding printing cycle. Without any real-time feedback control, the proposed STILC method can adjust T_u to reduce the difference between T_u and T_r. As a result, the slippage can be eliminated.

Each rotation cycle of the rewinding roller is defined as one iteration for the STILC method. The iterative updating law of the proposed STILC is a P-type ILC law described as the following:

$$u_{i+1}(\theta) = u_i(\theta) + \mathcal{L}\Phi(\theta)E_i \tag{6}$$

where i is the iteration index, $u_{i+1}(\theta)$ is the STILC control input when the phase angle of the rewinding roller is θ for the $(i+1)$th iteration (current iteration), $u_i(\theta)$ is the STILC control input at the same phase angle for the ith iteration (last iteration), $\mathcal{L}$ is the learning gain. $\Phi(\theta)$ is a pre-defined basis function. In this research, we select a constant-value function in terms of angle over $[0, 2\pi]$. Therefore, this basis function can be removed from the iterative updating law (6) for its effect can be integrated into the learning gain $\mathcal{L}$. Because the control input variable is constant during each iteration, the updating law can be described in the iteration domain:

$$u_{i+1} = u_i + \mathcal{L}E_i. \tag{7}$$

E_i is the registration error with the largest absolute value measured during the ith iteration, as described in (8):

$$E_i = TOF(e_{i1}, e_{i2}, e_{i3}) \tag{8}$$

where $TOF(\cdot)$ is the terminal output function that picks the registration error with the largest absolute value measured during one iteration, e_{i1}, e_{i2}, and e_{i3} are the three registration error measurements during the ith iteration, i.e.

$$\begin{aligned} e_{i1} &= \int_{\underline{\theta}_{i1}}^{\overline{\theta}_{i1}} R_r\, d\theta_r - \int_0^{2\pi} R_p\, d\theta_p \\ e_{i2} &= \int_{\underline{\theta}_{i2}}^{\overline{\theta}_{i2}} R_r\, d\theta_r - \int_{2\pi}^{4\pi} R_p\, d\theta_p \\ e_{i3} &= \int_{\underline{\theta}_{i3}}^{\overline{\theta}_{i3}} R_r\, d\theta_r - \int_{4\pi}^{6\pi} R_p\, d\theta_p \end{aligned} \tag{9}$$

where $\underline{\theta}_{i1}$ and $\overline{\theta}_{i1}$ are the phase angles of the rewinding roller in the ith iteration when the printing roller angle is going through 0 - 2π; $\underline{\theta}_{i2}$ and $\overline{\theta}_{i2}$ are the phase angles of the rewinding roller in the ith iteration when the printing roller angle is going through 2π - 4π; $\underline{\theta}_{i3}$ and $\overline{\theta}_{i3}$ are the phase angles of the rewinding roller in the ith iteration when the printing roller angle is going through 4π - 6π. It should be noted that the angular displacement of the printing roller θ_p is not synchronized with the angular displacement of the rewinding roller θ_r, and we use the latter to construct the iteration for our STILC design. In other words, the θ_r serves as θ in (6).

It should be noted that the P-type STILC updating law (6) is mathematically similar to a P-type run-to-run control law [48]. However, there are two main differences between them: (1) the run-to-run control in the given reference is model-based, whereas the STILC is model-free; (2) the run-to-run control is mainly applied in semiconductor manufacturing where in-situ metrology of product qualities is not always feasible. The control input u is a "recipe" adjusted offline during the stoppage time between two runs. However, in demonstrating our STILC method within the R2R printing process, there is no stoppage time between two iterations. The vision-based data are processed and then used to generate the feedforward control profile immediately following the termination of the last iteration.

3.2. Convergence analysis

In this section, we conduct a theoretical analysis of the stability of the controlled system. This analysis demonstrates that the registration error will converge to zero, provided certain assumptions are met. These findings offer reliable guidance for selecting an appropriate learning gain in designing the STILC updating law.

Given that the control input profile u keeps constant in a single iteration, and the registration error e measured at the end of the iteration is impacted by the control input profile and the iteration-wise uncertainty, we can write the relation between the E_i and u_i in ith iteration as the following lifted-form function:

$$E_i = g(u_i) + W_i \tag{10}$$

where u_i is a scalar and $g(\cdot)$ is a function of u_i. W_i is the uncertainty in ith iteration.

Assumption 5. The iteration-wise uncertainty W_i is bounded, i.e. $|W_i| < W_{max}$, where W_{max} is a positive constant.

The function $g(\cdot)$ can be derived from the time-domain system model described by (2)–(5), along with the terminal output function (8). It can be proved that $g(\cdot)$ exhibits certain properties, as elaborated in the following proposition.

Proposition 1. *The function $g(\cdot)$ satisfies the two properties below:*
(1) $[g(u_a) - g(u_b)](u_a - u_b) < 0$ for any $u_a \neq u_b$, and
(2) There exists a positive constant C satisfying $|g(u_a) - g(u_b)|/|u_a - u_b| > C$ for any $u_a \neq u_b$ when E_i is nonzero.

The proof of Proposition 1 is provided in the Supplementary Materials.

Utilizing Proposition 1 streamlines the following convergence analysis, enabling us to establish the theorem presented below.

Theorem 1. *For the registration error E_i described by (2)–(5) and the terminal output function (8), the proposed STILC law (7) can guarantee that registration error E_i converges to zero in the iteration domain, if Assumptions 1–5 and Proposition 1 hold, and $|1 - \mathcal{L}C| < 1$.*

Proof. Substituting (10) into (7), we get

$$u_{i+1} = u_i + Lg(u_i) + \mathcal{L}W_i. \tag{11}$$

Replacing i with $i - 1$ in (11), we further get

$$u_i = u_{i-1} + Lg(u_{i-1}) + \mathcal{L}W_{i-1}. \tag{12}$$

Subtracting (12) from (11), we have

$$\Delta u_i = \Delta u_{i-1} + \mathcal{L}[g(u_i) - g(u_{i-1})] + \mathcal{L}(W_i - W_{i-1}), \tag{13}$$

where $\Delta u_i = u_{i+1} - u_i$.

According to Assumption 4 and Proposition 1, (13) yields the following inequality

$$|\Delta u_i| \leq |\Delta u_{i-1}| - \mathcal{L}C|\Delta u_{i-1}| + 2\mathcal{L}W_{max}. \tag{14}$$

Obviously, when $|1 - \mathcal{L}C| < 1$ holds, it is guaranteed that $\lim_{i\to\infty} |\Delta u_i| = 0$, which means the control input u converges to a constant. From (7), we know $\Delta u_i = \mathcal{L}E_i$. Hence E_i converges to zero. ■

4. Experiment validation

4.1. Substrate material and ink

The polyethylene terephthalate (PET) substrate web was obtained from DuPont (Mylar Type A Polyester Film) and had a thickness of 50.8 μm. The Young's Modulus of the web is 4.8 GPa. The ink used in the experiment has a viscosity of 800 cP.

4.2. Online image processing

In order to quantify the dynamics occurring within each printing cycle, we have developed an online image sequence registration algorithm. This algorithm serves to calculate the displacements along both the machine and lateral directions of the R2R system. As illustrated in Fig. 3, our approach involves selecting small reference patches (depicted as red squares) and subsequently identifying all corresponding patches across the entire image. It is important to note that the identification process is initiated only when two valid patches are precisely found within the image. The essence of our methodology lies in computing the positional gap between these two valid patches. This specific gap signifies the substrate displacement that transpires during a single cycle of the gravure printing process. A comprehensive outline of the algorithm's intricacies can be found in Algorithm 1.

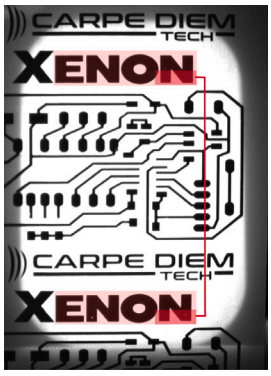

Fig. 3. Registration error computed from the positional gap between two small reference patches, highlighted in red.

Algorithm 1: Image Sequence Registration

Input: Images $\boldsymbol{I_k}$ from the camera sensor, $k = \{1, 2, 3 \cdots\}$;
Image $\boldsymbol{I_p}$ patch for registration;
Minimum searching range $\boldsymbol{D}$;
Matching threshold $\boldsymbol{Th}$.

Output: Top three Matched positions, $\boldsymbol{Pos}$;
The corresponding gap between two valid positions, $\boldsymbol{gap}$.

for $k \leftarrow 1$ *to* n **do**
  // Crop the central part of the original image
  $I_k \leftarrow crop(I_k)$
  // Find the normalized 2-D correlation matrix
  $c \leftarrow normxcorr2(I_p, I_k)$
  // Descending sorting
  $c \leftarrow sort(c)$
  Find the position $[\boldsymbol{xp1}, \boldsymbol{yp1}]$ with the value $\boldsymbol{c(1)}$
  Find the position $[\boldsymbol{xp2}, \boldsymbol{yp2}]$ with the value $\boldsymbol{c(2)}$
  $cnt \leftarrow 2$
  while $(xp2 - xp1)^2 + (yp2 - yp1)^2 \leq D^2$ **do**
    $cnt \leftarrow cnt + 1$
    Update $[\boldsymbol{xp2}, \boldsymbol{yp2}]$ to the value $\boldsymbol{c(cnt)}$
  end
  $cnt2 \leftarrow cnt$
  $[\boldsymbol{xp3}, \boldsymbol{yp3}] \leftarrow [\boldsymbol{xp2}, \boldsymbol{yp2}]$
  while $(xp2 - xp1)^2 + (yp2 - yp1)^2 \leq D^2$ *and* $(xp3 - xp1)^2 + (yp3 - yp1)^2 \leq D^2$ **do**
    $cnt \leftarrow cnt + 1$
    Update $[\boldsymbol{xp3}, \boldsymbol{yp3}]$ to the value $\boldsymbol{c(cnt)}$
  end
  $cnt3 \leftarrow cnt$
  $\boldsymbol{Pos(i)} \leftarrow [[\boldsymbol{yp1}, \boldsymbol{xp1}]; [\boldsymbol{yp2}, \boldsymbol{xp2}]; [\boldsymbol{yp3}, \boldsymbol{xp3}]]$
  // If only two valid matches, output the gap; otherwise, output [0,0]
  if $\boldsymbol{c(1)} \geq \boldsymbol{Th}$ *and* $\boldsymbol{c(cnt2)} \geq \boldsymbol{Th}$ *and* $\boldsymbol{c(cnt3)} < \boldsymbol{Th}$ **then**
    $\boldsymbol{gap(i)} \leftarrow [|\boldsymbol{yp2} - \boldsymbol{yp1}|, |\boldsymbol{xp2} - \boldsymbol{xp1}|]$
  else
    $\boldsymbol{gap(i)} \leftarrow \boldsymbol{[0, 0]}$
end

4.3. R2R gravure printing system

The proposed control algorithm was evaluated on an R2R gravure printing system as shown in Fig. 4. It consists of two subsystems:

the web handling system and the gravure printing module. The web handling system is composed of two motorized rollers and two idler rollers. A ring rotation encoder and a readhead were mounted on the rewinding roller to measure the linear web moving speed. The left idler roller is a tension measuring roller, which measures the tension of the moving web. The gravure printing module is where the printing process happens. The gravure printing module consists of an impression roller, a print roller, an ink tank, and a doctor blade. The print roller is a component in the printing process. Specifically, the anilox roller is engraved with tiny cells that store ink. These cells act as micro-caves, ensuring precise and consistent ink transfer onto the printing substrate. During printing, the print roller is partially immersed in the ink tank. As the roller rotates, the doctor blade scrapes the roller before it makes contact with the substrate, removing the excess ink from the non-printing areas and leaving the ink in the cells. Then, the web gets sandwiched between the impression roller and the print roller. The ink gets pulled out of the cell by the surface tension and transferred to the substrate. To ensure a balanced pressure between the impression roller and the print roller, a pressure control system is employed. The pressure is controlled by a step motor and a guide rail. To monitor the printing quality, an imaging system is installed. It consisted of a high-speed CMOS area-scan camera, a lighting source, and an objective lens. Additionally, An encoder was attached to the print roller to monitor the angle. The entire R2R gravure printing system is controlled by a real-time controller implemented with a Labview system.

4.4. Experiment procedure

The experiment was conducted in the following procedure. To synchronize the web moving speed and the gravure print roller speed, the two motorized rollers in the web handling system are controlled in torque mode. The print roller from the gravure printing module acts as the master speed roller. As a result, the web moves with the gravure print roller under the pressure between the impression roller and the print roller. To introduce the angle-periodic disturbance to the downstream web tension, an encoder was installed on the rewinding roller. It counts the rotation angle of the rewinding roller. Each time when the reading from the encoder is between 5°and 8°, the rewinding roller motor torque will have a sudden change to act as an impulse disturbance. As online image processing needs two consecutive repetitive patterns to appear in the same image, the camera has to be triggered carefully. In practice, another encoder is installed on the gravure printing roller and the camera is set to be triggered when the angle of this encoder is between 0 and 40°. Then, when the first two consecutive repetitive patterns appear in the same image, the encoder is reset to 0 degree. The image captured by the camera is fed into the image processing algorithm and the registration error is calculated accordingly. Based on the calculated registration error, the STILC will generate an input signal to adjust the torque of the unwinding roller motor, thereby compensating the registration error.

4.5. Experimental results

The experiment parameters are shown in Table 1. The radii of unwinding and rewinding rollers can be measured and other parameters are set in Labview. We test the performance of the system with three different disturbance magnitudes and STILC compensation. The STILC learning gain was obtained by tuning empirically. The experimental results are shown in Fig. 5. The angle-periodic impulse disturbances with different magnitudes are shown in Figs. 5(a)–5(c). Figs. 5(d)–5(f) show that STILC iteratively increases the value of unwinding roller motor torque to reduce the difference between the torques of unwinding and rewinding rollers. Figs. 5(g)–5(i) show the elimination of registration errors under different disturbances. We can observe the STILC-generated signals converge to a constant level and the registration errors are eliminated after no more than 10 iterations. These

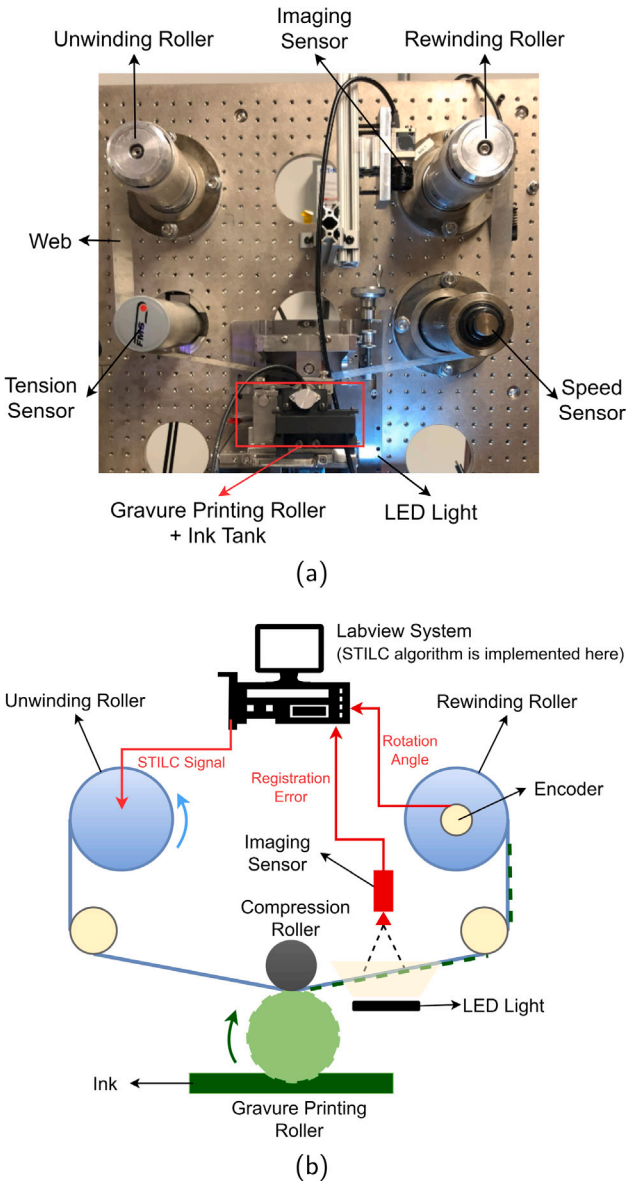

Fig. 4. Experimental Setup. (a) The experimental setup in the lab; (b) A scheme of the experimental setup.

Table 1
Experiment parameters.

Parameter	Notation	Value
Unwinding roller radius	R_u	0.0381 m
Rewinding roller radius	R_r	0.0381 m
Gravure printing roller speed	v_p	2.54 mm/s
Roller motor torque setpoint	T_u^r, T_r^r	1.144 N m
STILC learning gain	$\mathcal{L}$	15.12 N
Size of image I_k	–	1450 × 1100 pixels
Size of patch I_p	–	140 × 620 pixels
Normxcorr2 matching threshold	Th	0.7
Minimum searching range	D	100 pixels

experimental results are also consistent with the simulation results shown in our supplementary materials.

Additionally, we test the performance of the proposed STILC approach when the impulse disturbance magnitude varies online. As shown in Fig. 6(a), the disturbance magnitude is enlarged at the 7th and the 16th printing cycles. Before the disturbance magnitude is changed at the 6th and the 13th iterations, the registration error has been

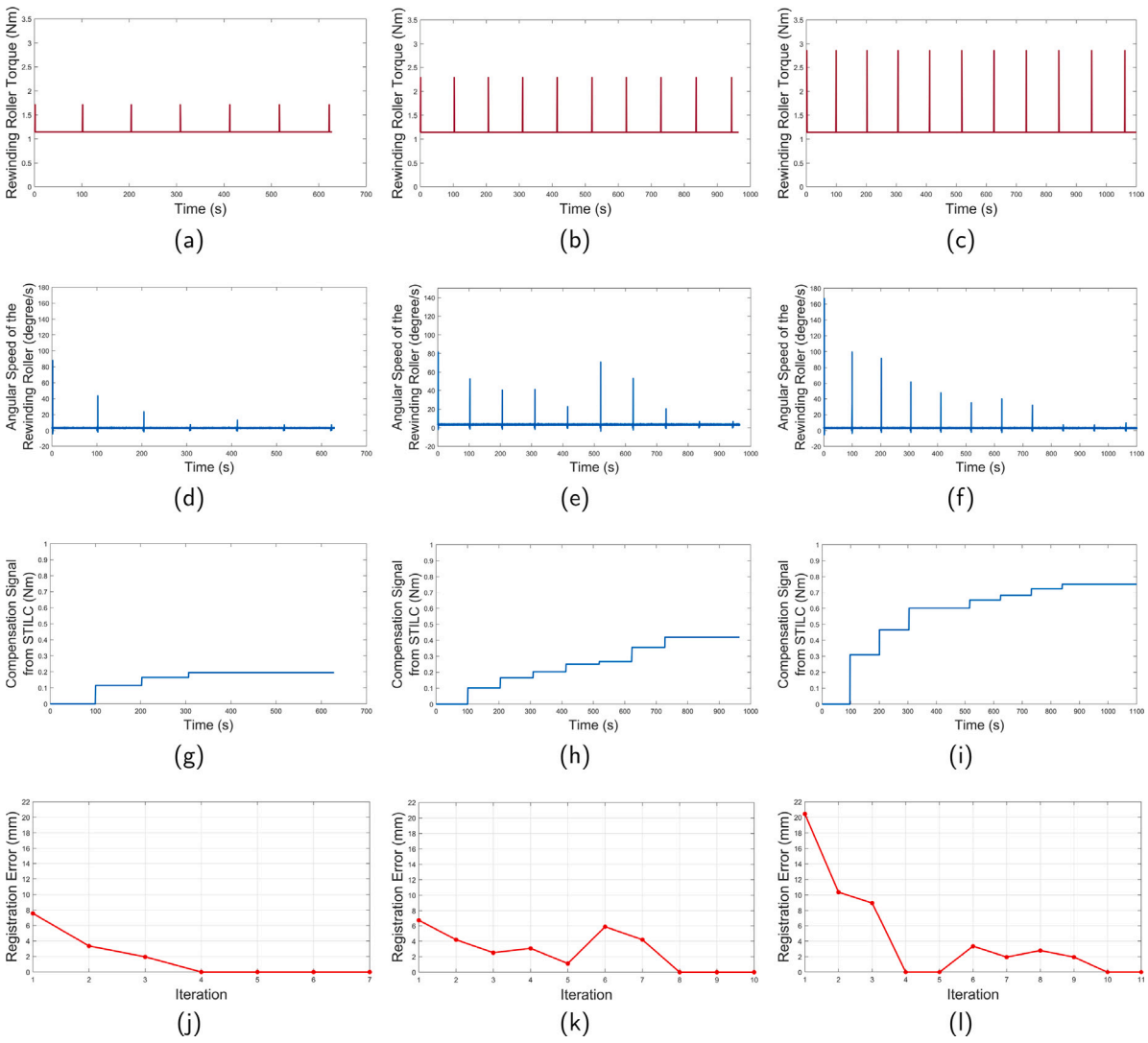

Fig. 5. Experiment results for small, medium, and large disturbance magnitudes. (a)–(c) are the disturbances with small, medium, and large impulse magnitudes; (d)–(f) are the angular speeds of the rewinding rollers when the disturbances are small, medium, and large; (g)–(i) are the STILC compensation signals when the disturbances are small, medium, and large; (j)–(l) are the registration error control performances when the disturbances are small, medium, and large.

eliminated. The changes generate registration errors in consequential iterations again, but the proposed STILC method shows timely responses to the varying disturbances and eliminates the registration error online. This experimental result is meaningful because the working conditions of R2R systems can be slowly varying in the iteration domain. For example, the radii of the unwinding and rewinding rollers are varying because the volume of the web wrapping on them is changing. Another example is the varying surface friction coefficient for the gravure printing roller because of the residual ink accumulation on the roller. Once the varying working conditions break the equilibrium state and result in new registration errors again, the proposed STILC is capable of responding to it and bringing the system back to the equilibrium state.

To summarize, the experimental results shown in Figs. 5 and 6 validate the effectiveness of the proposed STILC approach in the lab-scale R2R system. During the printing process, it does not require any real-time monitoring of web tensions or web speeds. The registration error is only measured by the image-based sensor at the end of each printing cycle and is fed into STILC every iteration (two printing cycles), which significantly lowers the requirements on sensor hardware and computational capability. With STILC, the slippage-related registration error caused by angle-periodic transient disturbances can be suppressed automatically. The effect of suppressing web slippage can be observed in the images captured by the image-based sensor. Before applying STILC to the system, there is a slippage region marked by the red box in Fig. 7(a). When STILC is applied, the slippage region is eliminated after sufficient printing cycles, as shown in Fig. 7(b).

5. Conclusion and discussion

This paper presents a novel STILC approach to tackle a fundamental challenge in registration control within R2R gravure printing systems with repetitive transient disturbances and the inability to monitor the real-time registration error. The proposed method overcomes these difficulties by incorporating a TILC updating law with a constant basis function in the spatial domain, enabling iterative convergence of the registration error to zero. To evaluate the effectiveness of the proposed STILC approach, we conduct a numerical simulation and an experiment on a lab-scale R2R gravure printing system. To simulate it numerically in *Simulink*, we model the dynamics of the registration error and the R2R system and introduce angle-periodic transient disturbances to the system. The simulation results shown in our supplementary materials demonstrate that our method achieves convergence of the registration error to zero after a few printing cycles. In the experiments, we then specify the same parameters in the lab-scale R2R gravure printing system and introduce the same disturbances. The registration error is

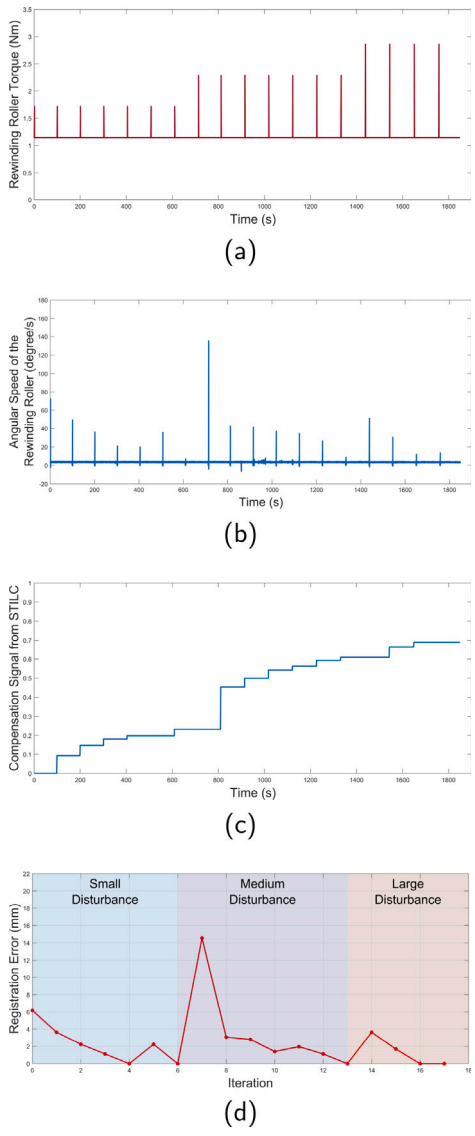

Fig. 6. Experiment results for online varying disturbances. (a) Disturbance; (b) Angular Speed; (c) STILC Signal; (d) Registration Error.

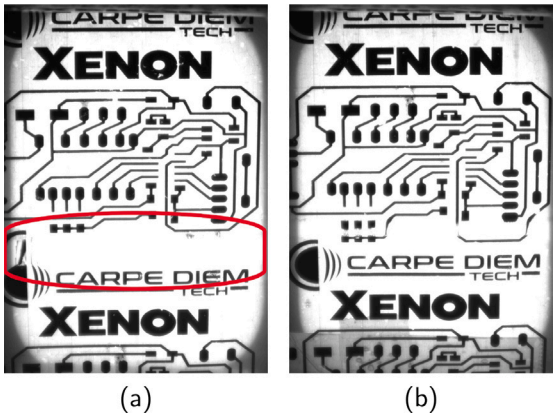

Fig. 7. The captured image at the end of one printing cycle when (a) there is a slippage; (b) there is no slippage.

measured by an image-based sensor and the online image processing algorithm. The experiment results shown in Fig. 5 are consistent with the performance we observed in the simulation results. The web slippages caused by the repetitive impulse disturbances are eliminated by the STILC compensation. Furthermore, we show that the proposed STILC can also adjust its compensation signal when the impulse disturbance magnitude is varying online and maintain the registration error at a relatively low level.

It is worth noting that the friction dynamics between the web and the roller is a sophisticated rolling friction dynamics and the slippage effect can also be complex, including both gaps (a part of pattern is missing) and overprints (a part of the pattern is overlapped in the same area). In this study, we measure the pitch length of the printed pattern and utilize it as an indicator of registration error. This approach is a compromise, chosen due to the limitations of our sensing capabilities. In future work, further investigation is needed to enhance the vision-based sensing system, making it capable of identifying more specific slippage regions and slippage classes, such as gap or overprint.

Furthermore, this work is demonstrated on a lab-scale experimental R2R setup, which means that some necessary adjustments could be needed if the proposed STILC method is applied to the industry-scale R2R systems. For industrial systems, the radius of the rewind roller increases as the substrate accumulates. Although the radius can be measured using a displacement sensor, the maximum force applied to the substrate diminishes as the roller radius grows. Therefore, we must ensure that the motor maintains sufficient torque to transport the substrate effectively. Further research is required to scale the application of STILC to industrial contexts.

CRediT authorship contribution statement

Zifeng Wang: Writing – review & editing, Writing – original draft, Visualization, Validation, Methodology, Formal analysis, Conceptualization. **Jingyang Yan:** Writing – original draft, Validation, Software, Formal analysis, Data curation. **Rui Ma:** Writing – original draft, Visualization, Validation. **Xian Du:** Writing – review & editing, Supervision, Resources, Project administration, Investigation, Funding acquisition. **Xiaoning Jin:** Writing – review & editing, Supervision, Resources, Project administration, Investigation, Funding acquisition.

Declaration of competing interest

The authors declare that they have no known competing financial interests or personal relationships that could have appeared to influence the work reported in this paper.

Acknowledgments

This material is derived from research supported by the National Science Foundation, United States under grants CMMI-1907250 and CMMI-1942185. The authors acknowledge Roll-to-Roll Fabrication and Processing Facility at UMass Amherst for partially offering gravure print head and ink. Dr. Jefferey Morse and Barbara Stewart offered advice on setting up and conducting ink on the gravure printing process.

Appendix A. Supplementary data

Supplementary material related to this article can be found online at https://doi.org/10.1016/j.jmapro.2025.06.004.

References

[1] Jeong H, Noh Y, Kim J, Ko S, Lee D. Sequential manufacturing via intra-additive hybrid materials approach for fully roll-to-roll processed flexible organic thin film transistors. J Manuf Process 2021;72:138–47. http://dx.doi.org/10.1016/j.jmapro.2021.10.001, URL: https://www.sciencedirect.com/science/article/pii/S1526612521007209.

[2] Chen C-M, Anastasova S, Zhang K, Rosa BG, Lo BPL, Assender HE, Yang G-Z. Towards wearable and flexible sensors and circuits integration for stress monitoring. IEEE J Biomed Heal Inform 2020;24(8):2208–15. http://dx.doi.org/10.1109/JBHI.2019.2957444.

[3] Kwon S, Song D, Kim H, Lee M, Woo K. Development of roll-to-roll multi-layer thermal evaporation system for flexible OLED devices. In: 2018 25th international workshop on active-matrix flatpanel displays and devices. AM-FPD, 2018, p. 1–2. http://dx.doi.org/10.23919/AM-FPD.2018.8437386.

[4] Wood III DL, Wood M, Li J, Du Z, Ruther RE, Hays KA, Muralidharan N, Geng L, Mao C, Belharouak I. Perspectives on the relationship between materials chemistry and roll-to-roll electrode manufacturing for high-energy lithium-ion batteries. Energy Storage Mater 2020;29:254–65.

[5] Di Giacomo F, Fledderus H, Gorter H, Kirchner G, de Vries I, Dogan I, Verhees W, Zardetto V, Najafi M, Zhang D, et al. Large area >140 cm^2 perovskite solar modules made by sheet to sheet and roll to roll fabrication with 14.5% efficiency. In: 2018 IEEE 7th world conference on photovoltaic energy conversion (WCPEC) (a joint conference of 45th IEEE PVSC, 28th PVSEC & 34th EU PVSEC). IEEE; 2018, p. 2795–8.

[6] Zuo C, Scully AD, Vak D, Tan W, Jiao X, McNeill CR, Angmo D, Ding L, Gao M. Self-assembled 2D perovskite layers for efficient printable solar cells. Adv Energy Mater 2019;9(4):1803258.

[7] Zuo C, Scully AD, Gao M. Drop-casting method to screen Ruddlesden–Popper perovskite formulations for use in solar cells. ACS Appl Mater Interfaces 2021;13(47):56217–25.

[8] Shakeel A, Maskey BB, Shrestha S, Parajuli S, Jung Y, Cho G. Towards digital twin implementation in roll-to-roll gravure printed electronics: Overlay printing registration error prediction based on printing process parameters. Nanomaterials 2023;13(6):1008.

[9] Chen J, Liu H, Huang Y, Yin Z. High-rate roll-to-roll stack and lamination of multilayer structured membrane electrode assembly. J Manuf Process 2016;23:175–82. http://dx.doi.org/10.1016/j.jmapro.2016.06.022, URL: https://www.sciencedirect.com/science/article/pii/S1526612516300792.

[10] Kim C, Jeon SW, Kim CH. Measurement of position accuracy of engraving in plate roller and its effect on register accuracy in roll-to-roll multi-layer printing. Meas Sci Technol 2017;28(12):125002.

[11] Lee J, Park S, Shin K-H, Jung H. Smearing defects: A root cause of register measurement error in roll-to-roll additive manufacturing system. Int J Adv Manuf Technol 2018;98(9):3155–65.

[12] Jabbar KA, Pagilla PR. Modeling and analysis of web span tension dynamics considering thermal and viscoelastic effects in roll-to-roll manufacturing. J Manuf Sci Eng 2018;140(5):051005.

[13] Chen Z, Zhang T, Zheng Y, Wong DS-H, Deng Z. Fully decoupled control of the machine directional register in roll-to-roll printing system. IEEE Trans Ind Electron 2021;68(10):10007–18. http://dx.doi.org/10.1109/TIE.2020.3029476.

[14] Chen Z, Zheng Y, Zhang T, Wong DS-H, Deng Z. Modeling and register control of the speed-up phase in roll-to-roll printing systems. IEEE Trans Autom Sci Eng 2018;16(3):1438–49.

[15] Kang H, Lee C, Shin K. Modeling and compensation of the machine directional register in roll-to-roll printing. Control Eng Pract 2013;21(5):645–54.

[16] Seshadri A, Pagilla PR, Lynch JE. Modeling print registration in roll-to-roll printing presses. J Dyn Syst Meas Control 2013;135(3):031016.

[17] Shi J. The interaction between webs and rollers in roll-to-roll manufacturing process machines [Ph.D. thesis], Oklahoma State University; 2019.

[18] Chen Z, Qu B, Jiang B, Forrest SR, Ni J. Robust constrained tension control for high-precision roll-to-roll processes. ISA Trans 2023;136:651–62. http://dx.doi.org/10.1016/j.isatra.2022.11.020, URL: https://www.sciencedirect.com/science/article/pii/S0019057822006127.

[19] Shah K, He A, Wang Z, Du X, Jin X. Data-driven model predictive control for roll-to-roll process register error. In: International manufacturing science and engineering conference. vol. 86601, American Society of Mechanical Engineers; 2022, V001T03A006.

[20] Pagilla PR, Siraskar NB, Dwivedula RV. Decentralized control of web processing lines. IEEE Trans Control Syst Technol 2006;15(1):106–17.

[21] Yan J, Du X. Neural-network-based adaptive model predictive control for a flexure-based roll-to-roll contact printing system. IEEE/ASME Trans Mechatronics 2022;27(6):5084–94.

[22] Bristow DA, Tharayil M, Alleyne AG. A survey of iterative learning control. IEEE Control Syst Mag 2006;26(3):96–114.

[23] Yu C, Ma J, Pan H, Basin MV. Adaptive iterative learning constrained control for linear-motor-driven gantry stage. IEEE/ASME Trans Mechatronics 2024;29(3):1647–58. http://dx.doi.org/10.1109/TMECH.2023.3312120.

[24] Sutanto E, Alleyne AG. Norm optimal iterative learning control for a roll to roll nano/micro-manufacturing system. In: 2013 American control conference. IEEE; 2013, p. 5935–41.

[25] Sutanto E, Alleyne AG. Vision based iterative learning control for a roll to roll micro/nano-manufacturing system. IFAC Proc Vol 2014;47(3):7202–7.

[26] Lee J, Seong J, Park J, Park S, Lee D, Shin K-H. Register control algorithm for high resolution multilayer printing in the roll-to-roll process. Mech Syst Signal Process 2015;60:706–14.

[27] Wang Z, Jin X. An adaptive spatial-terminal iterative learning strategies in roll-to-roll control problems. In: ASME international mechanical engineering congress and exposition. vol. 88605, American Society of Mechanical Engineers; 2024, V002T03A104.

[28] Han J, Shen D, Chien C-J. Terminal iterative learning control for discrete-time nonlinear system based on neural networks. In: 2015 34th Chinese control conference. CCC, 2015, p. 3190–5. http://dx.doi.org/10.1109/ChiCC.2015.7260132.

[29] Bu X, Liang J, Hou Z, Chi R. Data-driven terminal iterative learning consensus for nonlinear multiagent systems with output saturation. IEEE Trans Neural Netw Learn Syst 2021;32(5):1963–73. http://dx.doi.org/10.1109/TNNLS.2020.2995600.

[30] Chi R, Wang D, Hou Z, Jin S. Data-driven optimal terminal iterative learning control. J Process Control 2012;22(10):2026–37.

[31] Xu J-X, Chen Y, Lee TH, Yamamoto S. Terminal iterative learning control with an application to RTPCVD thickness control. Automatica 1999;35(9):1535–42.

[32] Sahoo S, Panda S, Xu J. Application of spatial iterative learning control for direct torque control of switched reluctance motor drive. In: 2007 IEEE power engineering society general meeting. IEEE; 2007, p. 1–7.

[33] Afkhami Z, Pannier C, Aarnoudse L, Hoelzle D, Barton K. Spatial iterative learning control for multi-material three-dimensional structures. ASME Lett Dyn Syst Control 2021;1(1):011011.

[34] Altın B, Wang Z, Hoelzle DJ, Barton K. Robust monotonically convergent spatial iterative learning control: Interval systems analysis via discrete Fourier transform. IEEE Trans Control Syst Technol 2018;27(6):2470–83.

[35] Wang Z, Pannier CP, Barton K, Hoelzle DJ. Application of robust monotonically convergent spatial iterative learning control to microscale additive manufacturing. Mechatronics 2018;56:157–65.

[36] Zhang Y, Yin M, Li W, Xiang J, Ding X. Layered and subregional control strategy based on model-free adaptive iterative learning for laser additive manufacturing process. J Manuf Process 2023;102:806–13. http://dx.doi.org/10.1016/j.jmapro.2023.07.080, URL: https://www.sciencedirect.com/science/article/pii/S1526612523007715.

[37] Liu Y, Ruan X. Spatial iterative learning control for pitch of wind turbine. In: 2018 IEEE 7th data driven control and learning systems conference. DDCLS, IEEE; 2018, p. 841–6.

[38] Li J, You Z, Li Y, Miao E, Yue R. Five-axis contour error control based on spatial iterative learning. IEEE Trans Autom Sci Eng 2023;20(1):112–23. http://dx.doi.org/10.1109/TASE.2022.3142565.

[39] Cichy B, Gałkowski K, Rauh A, Aschemann H. Iterative learning control of the electrostatic microbridge actuator. In: 2013 European control conference. ECC, IEEE; 2013, p. 1192–7.

[40] Cichy B, Gałkowski K, Rogers E. Iterative learning control for spatio-temporal dynamics using Crank–Nicholson discretization. Multidimens Syst Signal Process 2012;23(1):185–208.

[41] Wang Z, Jin X. High-precision overlay registration via spatial-terminal iterative learning in roll-to-roll manufacturing. 2025, arXiv preprint arXiv:2503.08835.

[42] Ma R, Du X. Closed-loop feedback registration for consecutive images of moving flexible targets. Appl Intell 2023;53(9):10647–67.

[43] Siami M, Khaburi DA, Rodriguez J. Torque ripple reduction of predictive torque control for PMSM drives with parameter mismatch. IEEE Trans Power Electron 2016;32(9):7160–8.

[44] Yue H, He H, Han M. Study on torsional vibration characteristics and suppression of electric vehicles with dual-motor drive system. J Franklin Inst 2023;360(1):380–402.

[45] Kitamura M, Enomoto Y, Kaneda J, Komuro M. Cogging torque due to roundness errors of the inner stator core surface. IEEE Trans Magn 2003;39(3):1622–5.

[46] Huang Y, Tao H, Chen Y, Rogers E, Paszke W. Point-to-point iterative learning control with quantised input signal and actuator faults. Internat J Control 2023;1–16.

[47] Zhou C, Tao H, Chen Y, Stojanovic V, Paszke W. Robust point-to-point iterative learning control for constrained systems: a minimum energy approach. Internat J Robust Nonlinear Control 2022;32(18):10139–61.

[48] Wang Y, Gao F, Doyle III FJ. Survey on iterative learning control, repetitive control, and run-to-run control. J Process Control 2009;19(10):1589–600.